Supporting Information

New model of CFTR proposes active channel-like conformation

James Dalton, Ori Kalid, Maya Schushan, Nir Ben Tal, Jordi Villà-Freixa

TOC

This material is available free of charge via the Internet at http://pubs.acs.org.

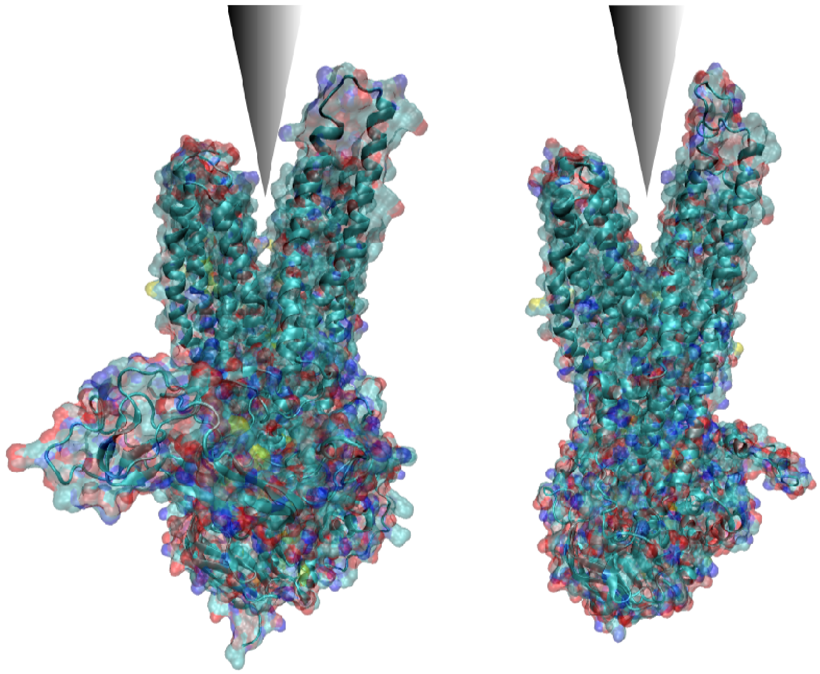

Figure S1. The homology models of Serohijos *et al*.[2] (left) and Mornon *et al*.[3] (right). The "outward-facing" conformation of both models results in an overly extended pore which does not reflect the experimentally proposed architecture.

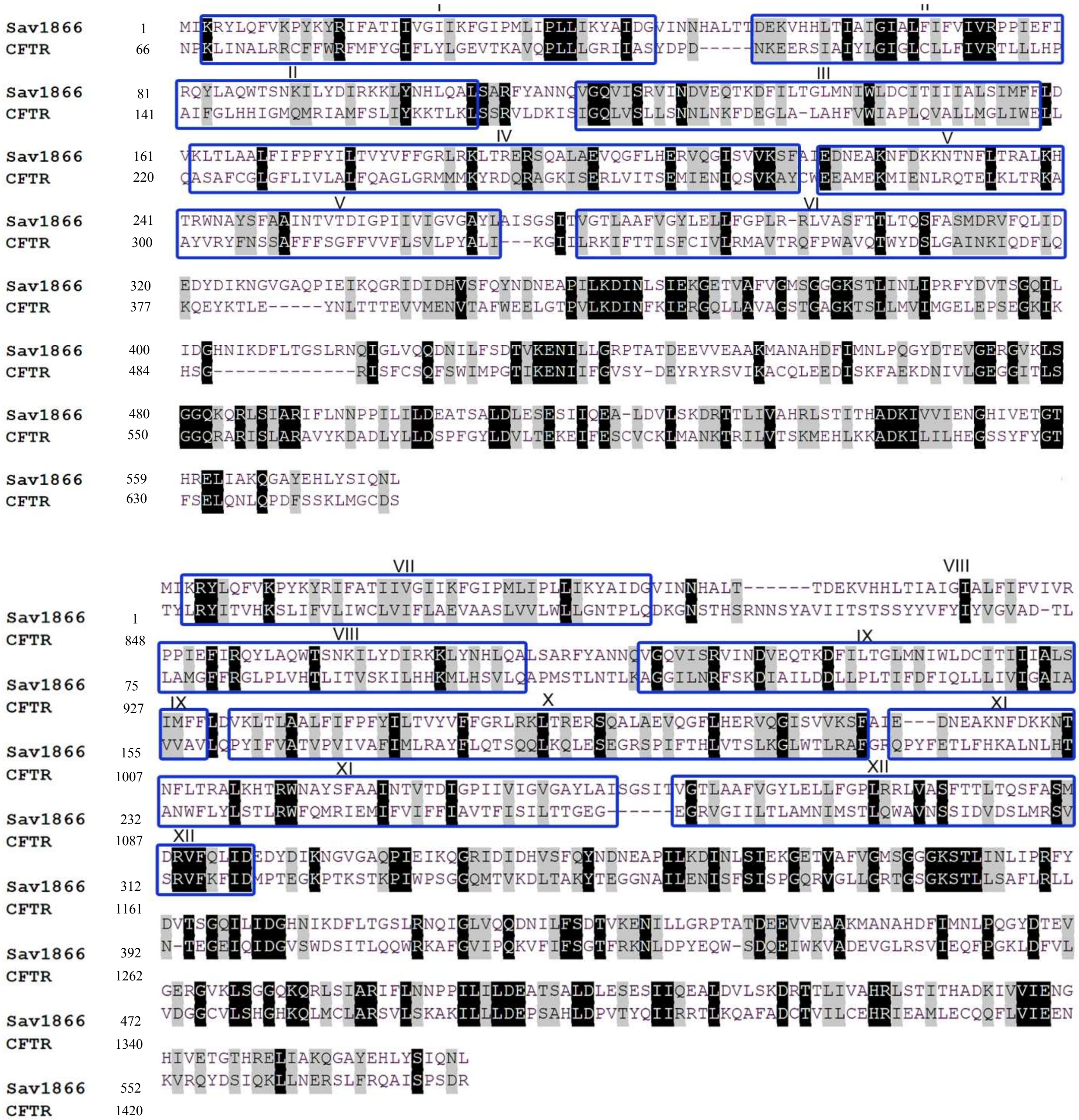

Figure S2. Sequence alignment of CFTR to Sav1866

Assignment of TM3, TM8 and TM11

The assignments of TM3, TM8 and TM11 were the most challenging. Profile-to-profile alignments uniformly predicted the boundaries for TM3, placing a single gap in the sequence of CFTR within the suggested segment, despite differences in the exact position of the gap. Examining hydrophobicity and conservation, we decided to place the gap before L198, approximately at the membrane boundary, ensuring that the majority of highly conserved and polar residues in TM3 do not face the membrane, as shown by Consurf[1] calculations in Figure S3.

The initial assignment of TM8 was in agreement with the expected conservation pattern. However, this assignment also oriented D924 towards the membrane, which is energetically disfavored and conflicts with experimental data, suggesting a salt bridge between D924 and R347[4]. To resolve this discrepancy, the first residue of TM8 was shifted one residue downstream and a gap was inserted in the pairwise alignment directly after D924, effectively rotating the side chain by ~100° toward the core of the TM bundle. This gap was modeled with helical constraints within MODELLER to ensure maintenance of helical structure. Although the insertion of this gap was not enough for salt bridge formation in itself, it provided improved starting conditions for subsequent refinement, ultimately resulting in salt bridge formation. Interestingly, the equivalent region in Sav1866 possesses two sequential prolines, suggesting that this region of TM8 may be distorted, and providing justification for inserting a gap in the pairwise alignment. The resulting TM8 alignment remained in agreement with the conservation pattern as calculated by Consurf (Figure S4).

In the case of TM11, the assignment suggested by all profile-to-profile alignments placed the relatively hydrophilic segment between S1094 and R1102 inside the membrane core, while the more hydrophobic region stretching from I1119 to G1123 was positioned outside the membrane at the extracellular side. Moreover, this caused the highly conserved R1102 to face the lipid tails, approximately one helical turn above the membrane boundary, which is counter-intuitive. Inserting three gaps in the former assignment shifted the helix three residues upstream (corresponding to residues: P1072, Y1073, F1074), offering a potential solution to these inconsistencies. Again, this region was modeled with relevant helical constraints within MODELLER to ensure maintenance of the helical structure of TM11 and ICL4.

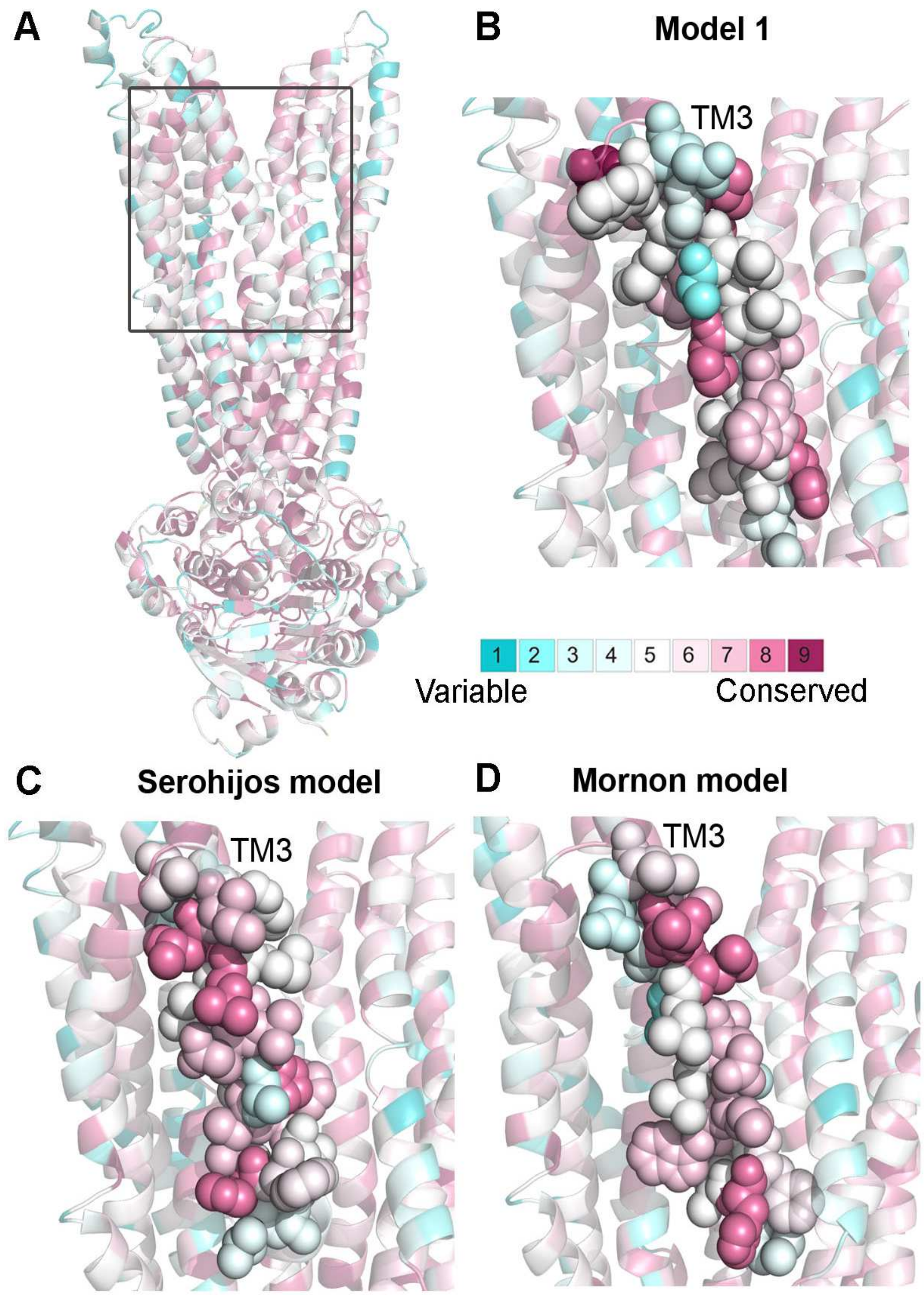

Figure S3. Different assignments of TM3 in light of evolutionary conservation. The models are colored by evolutionary conservation according to the Consurf[1] color scale, and only the TMDs are shown for clarity. A) Overview of current orientation; (B-D) Side view of current model in its initial outward-facing conformation, Serohijos[2] and Mornon[3] models, respectively. All the helices, excluding TM3, are shown as transparent ribbons. The residues that were assigned the highest conservation scores (grades 8 and 9) in TM3 are depicted as spheres. In this case, the current model orients all conserved residues, except for Pro205, towards the core, in contrast to the previously published models.

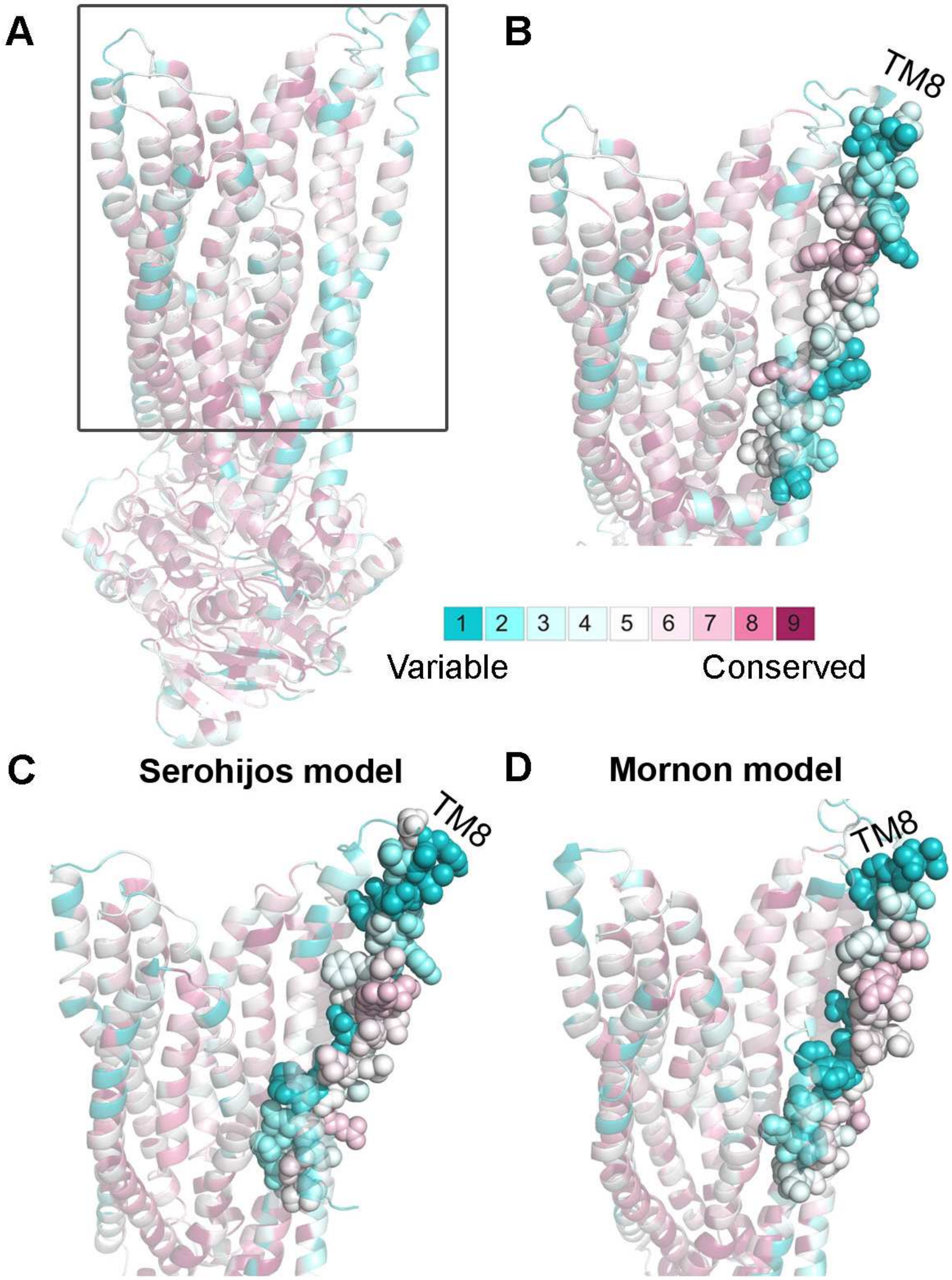

Figure S4. Different assignments of TM8 in light of evolutionary conservation. The models are colored by evolutionary conservation according to the Consurf[1] color scale, and only the TMDs are shown for clarity. A) Overview of current orientation; (B-D) Side views of current model in its initial outward-facing conformation, Serohijos[2] and Mornon[3] models, respectively. All the helices, excluding TM8, are shown as transparent ribbons. The residues that were assigned the highest conservation scores (grades 8 and 9) in TM8 are depicted as spheres. In contrast to the previously published models, most variable residues are facing the membrane.

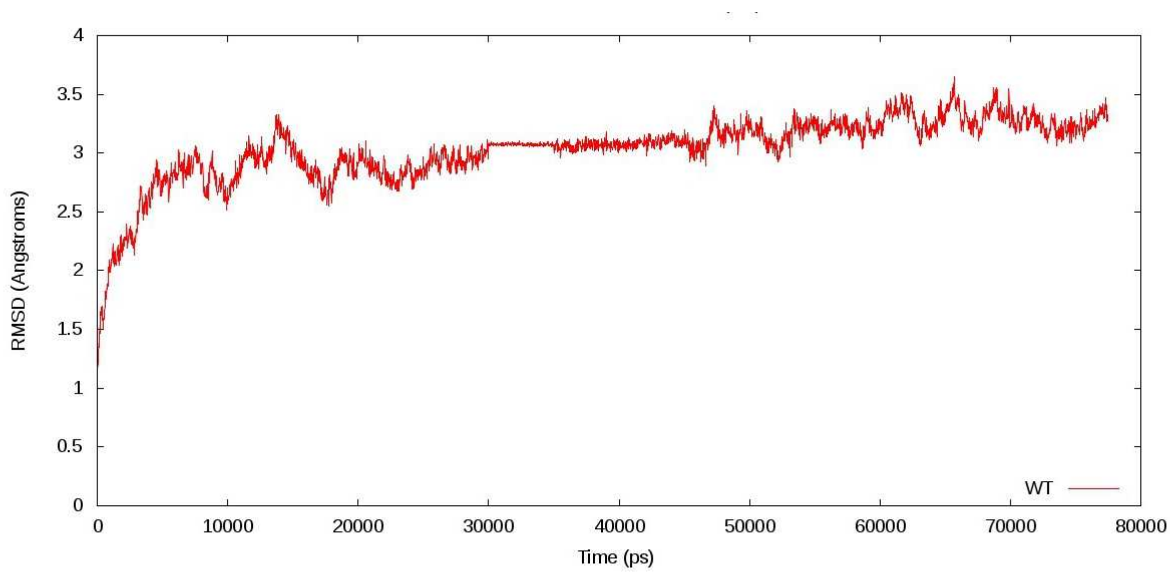

Figure S5. RMSD of the TM region (Cα atoms) of *wt* CFTR calculated over a 75ns MD trajectory, starting from the initial relaxed structure. The backbone of the TMs stabilizes over the course of the simulation, suggesting convergence may have been reached. The first phase of the simulation (0-30 ns) contains the constrained Cl^- column. In the second phase (30-45 ns), the Cl^- column is annihilated and replaced with unconstrained water molecules during an equilibration period (protein constraints are applied and gradually released). The third phase (45-75 ns) of the simulation is constraint-free.

Table S1: existence of experimentally proposed salt-bridges and hydrogen-bonds

Salt bridge	Ref	Serohijos outward facing model[2]	Mornon outward facing model[3]	Current "conducting state" model	Current model after MD (75ns simulation)
R347(TM6) – D924 (TM8)	4	No	Yes	Yes	Yes
R352 (TM6) – D993 (TM9)	5	No	No	Yes	Yes
Hydrogen bond					
R555 (NBD1) – T1246 (NBD2)	6	No	No	Yes	Yes

Table S2: Inter-residue distances compared with experimental cross-linking data

Cross-linked residues	**Ref**	Reagent / Cross-linker*								CB-CB or CB-CA distances (Å)				**Comment**
		Cu(II)(o-phenanthroline)2 (7Å)	**M1M (3.9Å)**	**M3M (6.5Å)**	**M5M (9.1Å)**	**M8M (13Å)**	**M17M (24.7Å)**	**BMOe (8Å)**	**BMH (16Å)**	Serohijos outward-facing[2]	Mornon outward-facing[3]	Current model	Current model after MD (75ns simulation)	
95(TM1)-1141(TM12)	7	+	ND	ND	ND	ND	ND	ND	ND	19.1	10.7	6.3	10.2	
171(ICL1)-407(NBD1)	8		ND	ND		+	ND			20.8	14.0	12.8	14.7	
171(ICL1)-408(NBD1)	8		ND	ND		+	ND			22.8	12.9	14.6	17.1	
171(ICL1)-1261(NBD2)	8		-	-		-	-			30.0	38.5	40.1	38.9	
172(ICL1)-543(NBD2)	8		-	-		-	-			27.7	19.9	18.6	17.9	
172(ICL1)-1341(NBD2)	8		+	+		+	+			9.6	6.6	11.8	10.9	Flexible Loop
268(ICL2)-1294(NBD2)	8		+	+		+	+			5.1	4.1	5.6	4.7	Flexible Loop

268(ICL2)-1341(NBD2)	8		+	+		+	+			10.1	11.6	10.2	10.8	Flexible Loop
276(ICL2)-1280(NBD2)	2	+	+	+		+	+			5.3	4.0	5.3	4.8	Flexible Loop
276(ICL2)-1284(NBD2)	2		ND	+		+	+			6.6	5.1	4.5	6.5	Flexible Loop
276(ICL2)-1307(NBD2)	8		weak	+		+	weak			5.7	10.4	8.4	9.6	Flexible Loop
340(TM6)-877(TM7)	9		-	-	-	+	+	-		13.3	9.6	10.4	8.9	
348(TM6)-1142(TM12)	10				+	+	-			14.8	17.1	11.5	10.4	
351(TM6)-1142(TM12)	10				-	+	-			14.6	18.5	13.2	13.4	
356(TM6)-1145(TM12)	10				+	+	+			22.9	14.5	12.3	13.9	
408(NBD1)-961(ICL3)	8		-	-		-	-			48.0	33.6	32.6	32.1	
434(NBD1)-1336(NBD2)	11							-	+	13.5	20.5	19.3	19.6	
434(NBD1)-1374(NBD2)	11							-	-	23.9	31.8	33.9	32.6	
459(NBD1)-1248(NBD2)	11							-	-	29.9	32.7	31.0	31.6	
459(NBD1)-1379(NBD2)	11							+	+	7.3	6.5	5.9	5.7	
462(NBD1)-1347(NBD2)	11		weak					+	+	7.5	7.9	8.3	8.9	
496(NBD1)-1064(ICL4)	8		ND	+		+	+			4.1	4.5	5.9	6.2	Flexible Loop
496(NBD1)-1292(NBD2)	8		+	+		+	+			10.9	11.5	10.7	14.1	Flexible Loop
498(NBD1)-1061(ICL4)	8		+	+		+	+			7.7	8.6	9.1	5.9	Flexible Loop
498(NBD1)-1065(ICL4)	8		ND	+		+	+			7.5	10.1	10.4	9.7	Flexible Loop
508(NBD1)-1065(ICL4)	2		ND	+		+	+			7.0	7.8	7.3	8.3	
508(NBD1)-1068(ICL4)	2	-	weak	+		+	+			2.9	5.7	7.1	7.5	
508(NBD1)-1069(ICL4)	2	-	weak	+		+	+			7.0	9.8	10.1	11.4	
508(NBD1)-1074(ICL4)	2		ND	+		+	+			7.6	8.9	6.6	12.1	
510(NBD1)-1069(ICL4)	2	-	weak	+		+	+			6.2	10.9	9.9	11.8	Flexible Loop
543(NBD1)-966(ICL3)	8		+	+		+	+			10.9	7.6	11.2	10.5	Flexible Loop
543(NBD1)-1057(ICL4)	8		+	+		+	+			9.4	8.0	5.9	8.7	Flexible Loop
549(NBD1)-1248(NBD2)	11, 6	+						+	+	7.9	7.9	8.3	8.8	
549(NBD1)-1336(NBD2)	11							-	-	37.7	37.4	37.5	35.1	
549(NBD1)-1374(NBD2)	11							-	+	14.9	13.6	13.7	11.9	
549(NBD1)-1379(NBD2)	11							-	-	27.7	28.2	28.5	27.3	
564(NBD1)-1069(ICL4)	2		ND	weak		+	weak			4.6	10.2	7.0	10.1	
605(NBD1)-1336(NBD2)	11							-	-	30.9	28.8	30.7	33.5	
605(NBD1)-1374(NBD2)	11							+	+	9.8	7.9	7.8	12.0	
961(ICL3)-1260(NBD2)	8		+	+		+	+			4.1	4	4.4	7.8	Flexible Loop
961(ICL3)-1261(NBD2)	8		+	+		+	+			7.5	6.2	6.2	7.8	Flexible Loop

962(ICL3)-1261(NBD2)	8		+	+		+	+			4.0	6.4	4.9	6.7	Flexible Loop
966(ICL3)-1341(NBD2)	8		-	-		-	-			24.0	25.1	25.0	24.5	

ND: Not Determined

Red: Significantly contrasting with cross-linking data, i.e. model distance outside range of measured cross-linking distances. As CFTR is an inherently dynamic structure which also contains several flexible loop regions, multiple cross-linking distances may be possible in several locations.

*MXM cross linker spacer size estimates taken from Loo and Clarke 2001[12]; BMOe and BMH cross linker spacer size estimates taken from Mense, *et al* 2006[11]; Cu(II)(o-phenanthroline)^2 cross linker spacer size estimate taken from Stockner *et al.* 2009.[13]

Table S3: Functional and accessibility data of TM6 residues

TM/ ICL	Residue	Mutation	Functional Effect	Ref
TM6	I332	C	Inaccessible to covalent modification	14
TM6	I333	C	less reactive to MTS reagents in the open channel state	14
TM6	R334	C	MTSET reaction rate greater in closed state	15
			Reduced conductance; Covalent modification reveals that positive charge is critical; Reaction to MTS reagents is not state dependent.	11
			Reduced block of Cl^- conductance by $[Au(CN)_2]^-$	16
		T	No detectable Cl^- current	16
		K	Reduced single channel conductance; Reduced block of Cl^- conductance by $[Au(CN)_2]^-$	16, 17

		W/Q/ L/H	Reduced conductance	16
TM6	K335	C	Less reactive to MTS reagents in the open channel state	14
			Reactive to covalent modification	18
		A	No effect on SCN^- binding	19
			Reduced single channel conductance	17
		D/E	Reduced SCN^- binding; Modified anion selectivity; Increased $K_{1/2}$(IBMX)	19
TM6	I336	C	Slowly reactive, only to permeant probe $[Ag(Cn)_2]^-$	18
		A	Reduced single channel conductance	17
TM6	F337	C	Reactive only to permeant probes $[Ag(Cn)_2]^-$ and $[Au(Cn)_2]^-$	14, 18
		A	Reduced single channel conductance; Modified anion selectivity	17, 20
		S	Modified anion selectivity	20
TM6	T338	C	Accessible to covalent modification	14, 18
		A	Increased single channel conductance; Reduced block of Cl^- conductance by $[Au(CN)_2]^-$	17
		A/S	Increased conductance, Modified anion selectivity	21
		I/V/N	Decreased conductance; Modified anion selectivity	21
TM6	T339	A	Minor changes in selectivity to larger anions	22
		C	Slowly reactive, only to permeant probe $[Ag(Cn)_2]^-$	18
TM6	I340	C	Reactive only to permeant probe $[Ag(Cn)_2]^-$	18
TM6	S341	C	Limited accessibility to covalent modification	14, 18
		A	Changed anion selectivity	22
			Reduced conductance	23
			Decreased block by DPC and NPPB	23

		E	Abolished block by high concentrations of DPC; Abolished anion selectivity more than any other mutation tested	22
		T	Slightly altered anion selectivity	22
			Slightly decreased block by DPC	23
TM6	F342	C	Reactive only to permeant probe $[Ag(Cn)_2]^-$	18
TM6	C343		Unreactive to covalent modification	18
TM6	I344	C	Reactive only to permeant probes $[Ag(Cn)_2]^-$ and $[Au(Cn)_2]^-$	18
TM6	V345	C	Reactive only to permeant probe $[Ag(Cn)_2]^-$	18
TM6	L346	C	Unreactive to covalent modification	18
TM6	R347	C	Unreactive to covalent modification	18
TM6	M348	C	Reactive only to permeant probes $[Ag(Cn)_2]^-$ and $[Au(Cn)_2]^-$	18
TM6	A349	C	Reactive only to permeant probe $[Ag(Cn)_2]^-$	18
TM6	V350	C	Unreactive to covalent modification	18
TM6	T351	C	Unreactive to covalent modification	18
TM6	R352	A/Q	Open state destabilized	5
TM6	Q353	C	Reactive only to permeant probe $[Ag(Cn)_2]^-$	18

PL: Pore Lining
NPL: Non Pore Lining

Coordinates of the pre-MD CFTR model

Available at http://ibis.tau.ac.il/wiki/nir_bental/index.php/Trans-membrane_structure_prediction

References

(1) Landau, M.; Mayrose, I.; Rosenberg, Y.; Glaser, F.; Martz, E.; Pupko, T.; Ben-Tal, N. ConSurf 2005: the projection of evolutionary conservation scores of residues on protein structures. *Nucleic Acids Res*. **2005**, *33*, W299-W302.
(2) Serohijos, A.W.; Hegedus, T.; Aleksandrov, A.A.; He, L.; Cui, L.; Dokholyan, N.V.; Riordan, J.R. Phenylalanine-508 mediates a cytoplasmic-membrane domain contact in the CFTR 3D structure crucial to assembly and channel function. *Proc Natl Acad Sci U S A*. **2008**, *105*, 3256-3261.
(3) Mornon, J.P.; Lehn, P.; Callebaut, I. Atomic model of human cystic fibrosis transmembrane conductance regulator: membrane-spanning domains and coupling interfaces. *Cell Mol Life Sci.* **2008**, *65*, 2594-2612.
(4) Cotten, J.F.; Welsh, M.J. Cystic fibrosis-associated mutations at arginine 347 alter the pore architecture of CFTR. *J Biol Chem.* **1999**, *274*, 5429-5435.
(5) Cui, G.; Zhang, Z. R.; O'Brien, A. R.; Song, B.; McCarty, N. A. Mutations at arginine 352 alter the pore architecture of CFTR. *J Membr Biol.* **2008**, *222*, 91-106.
(6) Vergani, P.; Lockless, S.W.; Nairn, A.C.; Gadsby, D.C. CFTR channel opening by ATP-driven tight dimerization of its nucleotide-binding domains. *Nature*. **2005**, *433*, 876-880.
(7) Zhou, J.J.; Li, M.S.; Qi, J.; Linsdell, P. Regulation of conductance by the number of fixed positive charges in the intracellular vestibule of the CFTR chloride channel pore. *The Journal of general physiology* **2010**, *135*, 229-245.
(8) He, L.; Aleksandrov, A.A.; Serohijos, A.W.; Hegedus, T.; Aleksandrov, L.A.; Cui, L.; Dokholyan, N.V.; Riordan, J.R. Multiple membrane-cytoplasmic domain contacts in the cystic fibrosis transmembrane conductance regulator (CFTR) mediate regulation of channel gating. *J Biol Chem*. **2008**, *283*, 26383-26390
(9) Wang, Y.; Loo, T.W.; Bartlett, M.C.; Clarke, D.M. Correctors promote maturation of cystic fibrosis transmembrane conductance regulator (CFTR)-processing mutants by binding to the protein. *J. Biol. Chem.* **2007**, *282*, 33247-33251.
(10) Chen, E.Y.; Bartlett, M.C.; Loo, T.W.; Clarke, D.M. The DeltaF508 mutation disrupts packing of the transmembrane segments of the cystic fibrosis transmembrane conductance regulator. *J Biol Chem.* **2004**, *279*, 39620-39627.
(11) Mense M.; Vergani, P.; White, D.M.; Altberg, G.; Nairn, A.C.; Gadsby, D.C. In vivo phosphorylation of CFTR promotes formation of a nucleotide-binding domain heterodimer. *EMBO J.* **2006**, *25*, 4728-4739.
(12) Loo, T.W.; Clarke, D.M. Determining the dimensions of the drug-binding domain of human P-glycoprotein using thiol cross-linking compounds as molecular rulers. *J Biol Chem*. **2001**, *276*, 36877-36880.
(13) Stockner T, de Vries SJ, Bonvin AM, Ecker GF, Chiba P. Data-driven homology modelling of P-glycoprotein in the ATP-bound state indicates flexibility of the transmembrane domains. *FEBS J.* **2009**, *276*, 964-972.
(14) Beck, E.J.; Yang, Y.; Yaemsiri, S.; Raghuram, V. Conformational changes in a pore-lining helix coupled to cystic fibrosis transmembrane conductance regulator channel gating. *J Biol Chem*. **2008**, *283*, 4957-4966.
(15) Zhang, Z.R.; Song, B.; McCarty, N.A. State-dependent Chemical Reactivity of an Engineered Cysteine Reveals Conformational Changes in the Outer Vestibule of the Cystic Fibrosis Transmembrane Conductance Regulator. *J Biol Chem.* **2005**, *280*, 41997-42003.
(16) Gong, X.; Linsdell, P. Maximization of the rate of chloride conduction in the CFTR channel pore by ion-ion interactions. *Arch Biochem Biophys.* **2004**, *426*, 78-82.
(17) Ge, N.; Muise, C.N.; Gong, X.; Linsdell, P. Direct comparison of the functional roles played by different transmembrane regions in the cystic fibrosis transmembrane conductance regulator chloride channel pore. *J Biol Chem.* **2004**, *279*, 55283-55289.
(18) Alexander, C.; Ivetac, A.; Liu, X.; Norimatsu, Y.; Serrano, J.R.; Landstrom, A.; Sansom, M.; Dawson, D. C. Cystic fibrosis transmembrane conductance regulator: using differential reactivity toward channel-permeant and channel-impermeant thiol-reactive probes to test a molecular model for the pore. *Biochemistry* **2009**, *48*, 10078-10088.
(19) Mansoura, M.K.; Smith, S.S.; Choi, A.D.; Richards, N.W.; Strong, T.V.; Drumm, M.L.; Collins, F.S.; Dawson, D.C. Cystic fibrosis transmembrane conductance regulator (CFTR) anion binding as a probe of the pore. *Biophys J.* **1998**, *74*, 1320-1332.

(20) Linsdell, P. Inhibition of cystic fibrosis transmembrane conductance regulator chloride channel currents by arachidonic acid. *Can J Physiol Pharmacol.* **2000**, *78*, 490-499.
(21) Linsdell, P.; Zheng, S.X.; Hanrahan, J.W. Non-pore lining amino acid side chains influence anion selectivity of the human CFTR Cl- channel expressed in mammalian cell lines. *J Physiol.* **1998**, *512*, 1-16.
(22) McCarty, N.A.; Zhang, Z.R. Identification of a region of strong discrimination in the pore of CFTR. *Am J Physiol Lung Cell Mol Physiol*. **2001**, *281*, L852-L867.
(23) McDonough, S.; Davidson, N.; Lester, H.A.; McCarty, N.A. Novel pore-lining residues in CFTR that govern permeation and open-channel block. *Neuron* **1994**, *13*, 623-634.